Chapter 4

86 GHz SiO maser survey of late-type stars in the Inner Galaxy III. Interstellar extinction and colours

M. Messineo, H. J. Habing, K. M. Menten, A. Omont,
L. O. Sjouwerman and F. Bertoldi

Abstract

We have computed extinction corrections for a sample of 441 late-type stars in the inner Galaxy using the 2MASS near-infrared photometry of the surrounding stars and assuming the intrinsic source colours. From this, the near-infrared power law is found to be $A_\lambda \propto \lambda^{-1.9\pm0.1}$. *Near- and mid-infrared colour-colour properties of known Mira stars are also reviewed. From the distribution of the dereddened infrared colours of the SiO target stars we infer mass-loss rates between* 10^{-7} *and* 10^{-5} $M_\odot$ yr^{-1}.

In this article we study the interstellar extinction toward a sample of evolved late-type stars in the inner Galaxy (-4° $< l <$ +30°, $|b| < 1°$) which were searched for SiO maser emission ("SiO targets" hereafter; Messineo et al. 2002, Chapter II). The maser emission reveals the stellar line of sight velocities with an accuracy of a few km s^{-1}, making the maser stars ideal for Galactic kinematics studies.

The combination of the kinematic information with the physical properties of the SiO targets, e.g. their intrinsic colours and bolometric magnitudes, will enable a revised kinematic study of the inner Galaxy, revealing which Galactic component and which epoch of Galactic star formation the SiO targets are tracing.

A proper correction for interstellar extinction is of primary importance for our photometric study of the stellar population of the inner Galaxy, where extinction can be significant even at infrared wavelengths. The extinction hampers an accurate determination of the stellar intrinsic colours and bolometric magnitudes.

This is especially critical in the central Bulge region where interstellar extinction is larger than 30 visual magnitudes and the uncertainty in the stellar bolo-

Astronomy and Astrophysics (2004), submitted

metric luminosities of evolved late-type stars is at least 1 magnitude due to the current uncertainty in the near-infrared extinction law (30%).

The available near- and mid-infrared photometry of the SiO targets from the DENIS[1] (Epchtein et al. 1994), 2MASS[2] (Cutri et al. 2003), ISOGAL[3] (Omont et al. 2003; Schuller et al. 2003) and MSX[4] (Egan et al. 1999; Price et al. 2001) surveys were already presented by Messineo et al. (2004b, Chapter III).

The corrections for interstellar extinction of the photometric measurements of each SiO target will enable us to derive the spectral energy distributions and bolometric magnitudes of the SiO targets. The bolometric magnitudes will be presented in a subsequent paper (Messineo et al. 2004a, Chapter V).

Our sample consists mainly of large-amplitude variable AGB stars (Chapter II; Chapter III). The estimates of interstellar extinction toward this class of objects are complicated by the presence of a circumstellar envelope which may have various thickness. Therefore, in order to disentangle circumstellar and interstellar extinction one needs to study the dust distribution along the line of sight toward each AGB star of interest. For each SiO target we adopt the median extinction derived from near-infrared field stars (mainly giants) close to the line of sight of the target. Then the dereddened colour-colour distribution of our targets is compared to those of local Mira stars in order to iteratively improve the extinction correction and to statistically estimate the mass-loss rates of our targets.

In Sect. 4.1 we discuss the uncertainty of the extinction law at near- and mid-infrared wavelengths, and the consequent uncertainty of the stellar luminosities. In Sect. 4.2 we describe the near-infrared colour-magnitude diagrams of field stars toward the inner Galaxy and we use the latter to derive the median extinction toward each target. In Sect. 4.3 we review the location of Mira stars on the colour-magnitude (CMD) and colour-colour diagrams. In Sects. 4.4 and 4.5 we use the median extinction from surrounding field stars to deredden our SiO targets and we discuss their colours and mass-loss rates. The main conclusions are given in Sect. 5.8.

4.1 Interstellar extinction law

The composition and abundance of interstellar dust and its detailed extinction properties remain unclear, limiting the accuracy of stellar population studies in the inner Galaxy. In the following we discuss the near- and mid-infrared extinction law, in order to assess the uncertainty in the extinction correction.

[1] DEep Near-Infrared Survey of the southern sky; see
`http://www-denis.iap.fr/`.
[2] Two Micron All Sky Survey; see
`http://www.ipac.caltech.edu/2mass/`.
[3] A deep survey of the obscured inner Milky Way with ISO at 7μm and at 15μm; see
`http://www-isogal.iap.fr/`.
[4] The Midcourse Space Experiment; see
`http://www.ipac.caltech.edu/ipac/msx/msx.html`.

4.1.1 Near-infrared interstellar extinction

Interstellar extinction at near-infrared wavelengths (1-5 μm) is dominated by graphite grains. Although for historical reasons the near-infrared extinction law is normalised in the visual, practically it is possible to derive near-infrared extinction by measuring the near-infrared reddening of stars of known colour.

Near-infrared photometric studies have shown that the wavelength-dependence of the extinction may be expressed by a power law, $A_\lambda \propto \lambda^{-\alpha}$, where α was found to range between 1.6 (Rieke & Lebofsky 1985) and 1.9 (Glass 1999; Landini et al. 1984; van de Hulst 1946).

When deriving the extinction from broad-band photometric measurements, one needs to properly account for the bandpass, stellar spectral shape, and the wavelength-dependence of the extinction. We have therefore computed an "effective extinction" for the DENIS I and 2MASS J, H and $K_{\rm s}$ passbands, as a function of the $K_{\rm S}$ band extinction. This effective extinction was computed by reddening an M0 III stellar spectrum (Fluks et al. 1994) with a power law extinction curve and integrating it over the respective filter transmission curves. When we convolve the filter response with a stellar sub-type spectrum different from the M0 III, the effective I-band extinction slightly differs, e.g. decreasing by 3% for a M7 III spectrum (see also van Loon et al. 2003).

The $K_{\rm S}$-band extinction $A_{\rm K_S}$ can then be found from

$$A_{\rm K_s} = C_{JK} \times E(J-K_{\rm s}),$$

$$A_{\rm K_s} = C_{HK} \times E(H-K_{\rm s}),$$

where $E(J-K_{\rm s})$ and $E(H-K_{\rm s})$ are the reddening in the $J-K_{\rm s}$ and $H-K_{\rm s}$ colour, respectively, and the C are constants. These relations are independent of visual extinction and of the coefficient of selective extinction, $R_{\rm V} = A_{\rm V}/E(B-V)$, but they depend on the slope of the near-infrared power law (see Table 4.1). However, to provide the reader with the traditionally used ratios between near-infrared effective extinction and visual extinction, we also used the commonly adopted extinction law of Cardelli et al. (1989). Such ratios may be useful in low-extinction Bulge windows, where visual data are also available. Cardelli et al. (1989) proposed an analytic expression, which depends only on the parameter $R_{\rm V}$, based on multi-wavelength stellar colour excess measurements from the violet to 0.9μm, and extrapolating to the near-infrared using the power law of Rieke & Lebofsky (1985). We extrapolated Cardelli's extinction law to near-infrared wavelengths using a set of different power laws. The results are listed in Table 4.1.

The uncertainty in the slope of the extinction law produces an uncertainty in the estimates of the near-infrared extinction of typically 30% in magnitude (see Table 4.1). For a $K_{\rm S}$ band extinction of $A_{\rm K_S}$= 3 mag the uncertainty may be up to 0.9 mag, which translates into an uncertainty in the stellar bolometric magnitudes of the same magnitude.

In Sect. 4.2 we show that a power law index $\alpha = 1.6$ is inconsistent with the observed colours of field giant stars toward the inner Galaxy, and that the most

likely value of α is 1.9 ± 0.1.

4.1.2 Mid-infrared interstellar extinction

Mid-infrared extinction (5-25 μm) is characterised by the 9.7 and 18 μm silicate features. The strength and profile of these features are uncertain and appear to vary from one line of sight to another. In the inner Galaxy silicate grains may be more abundant due to the outflows from oxygen-rich AGB stars. Another uncertainty is the minimum of $A_\lambda/A_{2.12}$ at 7μm, which is predicted for standard graphite-silicate mixes, though not observed to be very pronounced toward the Galactic Centre (Lutz 1999; Lutz et al. 1996).

The commonly adopted mid-infrared extinction curve is that of Mathis (1990), which is a combination of a power law and the astronomical silicate profile from Draine & Lee (1984), with $A_{9.7}/A_{2.2} \simeq 0.54$ – a value found in the diffuse interstellar medium toward Wolf-Rayet stars (e.g. Mathis 1998, and references therein). However, using hydrogen recombination lines, Lutz (1999) found $A_{9.7}/A_{2.2} \simeq 1.0$ in the direction of the Galactic centre, and analysing the observed H_2 level populations toward Orion OMC-1, Rosenthal et al. (2000) derived $A_{9.7}/A_{2.12} = 1.35$. It seems that the mid-infrared extinction law is not universal.

In order to derive the extinction ratios for all ISOGAL and MSX filters (for definitions see Blommaert et al. 2003; Price et al. 2001), and to analyse the effect of an increase of the depth of the 9.7 μm silicate feature on the extinction ratios, we built a set of extinction curves with different silicate peak strengths at 9.7 μm. We use a parametric mid-infrared extinction curve given by Rosenthal et al. (2000), where the widths of the 9.7 and 18 μm silicate features are those calculated by Draine & Lee (1984) and the depth of the 18 μm feature is assumed to be 0.44 times that of the 9.7 μm feature. Using this parametric fit we constructed two different extinction curves with $A_{9.7}/A_{2.2}$ equal to 1.0, one in combination with the minimum predicted by the models at 4-8 μm (Curve 2) and one without it as suggested by Lutz (1999) (Curve 3). The two curves are shown together with the Mathis curve (Curve 1, $A_{9.7}/A_{2.2} = 0.54$) in Fig. 4.1.

Using the various extinction curves detailed in Table 4.2, we reddened the M-type synthetic spectra from Fluks et al. (1994) (beyond 12.5μm a blackbody extrapolation is used), and convolved the resulting spectra with the ISOCAM and MSX filter transmission curves. The effective extinctions $\langle A \rangle / A_{\mathrm{K_S}}$ in the various ISOCAM and MSX filters are listed in Table 4.2. They are not sensitive to the stellar sub-type used. An increase of the ratio $A_{9.7}/A_{2.2}$ from 0.54 to 1.0 results in an increase between 0.15 and 0.20$\times A_{\mathrm{K_S}}$ of the average attenuation in the $LW3,\ LW9,\ C,\ D$ and E spectral bands. The spectral bands of the $LW2$ and $LW5$ filters are not very sensitive to the intensity of the silicate feature, but to the minimum of the extinction curve in the 4-8 μm region. Although $\langle A \rangle / A_{\mathrm{K_S}}$ varies with $A_{\mathrm{K_S}}$, these variations are small compared to those arising from different choices of the mid-infrared extinction law.

Hennebelle et al. (2001) obtained observational constraints on mid-infrared extinction ratios from observations of infrared dark clouds within the ISOGAL sur-

Table 4.1: *Near-infrared effective extinction, $\langle A \rangle / A_V \propto \lambda^{-\alpha}$, for various filters. A different value of R_V does not affect $A_{K_s}/E(H-K_s)$ and $A_{K_s}/E(H-K_s)$, but the slope of the extinction curve does. Our findings favour a model with $\alpha = 1.9$ (see Sect. 4.2).*

A_I/A_V	A_J/A_V	A_H/A_V	A_{K_S}/A_V	$A_{K_S}/E(J-K_s)$	$A_{K_s}/E(H-K_s)$	α	R_V	Ref.
0.592	0.256	0.150	0.089	0.533	1.459	1.85		Glass (1999)
0.584	0.270	0.165	0.103	0.617	1.661	1.73	3.08	He et al. (1995)
0.482	0.282	0.175	0.112	0.659	1.778	1.61	3.09	Rieke & Lebofsky (1985)
0.606	0.287	0.182	0.118	0.696	1.842	1.61	3.10	Cardelli et al. (1989)
0.563	0.259	0.164	0.106	0.696	1.842	1.61	2.50*	″
0.606	0.277	0.169	0.106	0.623	1.684	1.73	3.10	Cardelli et al. (1989)+
0.563	0.249	0.152	0.096	0.623	1.684	1.73	2.50	″
0.606	0.267	0.158	0.096	0.561	1.548	1.85	3.10	″
0.563	0.240	0.142	0.086	0.561	1.548	1.85	2.50	″
0.606	0.263	0.153	0.092	0.537	1.496	1.90	3.10	″
0.563	0.237	0.138	0.083	0.537	1.496	1.90	2.50	″
0.606	0.255	0.144	0.084	0.493	1.401	2.00	3.10	″
0.563	0.229	0.130	0.076	0.494	1.400	2.00	2.50	″
0.606	0.238	0.127	0.070	0.420	1.236	2.20	3.10	″
0.563	0.213	0.114	0.063	0.420	1.236	2.20	2.50	″

* recent determination toward the Bulge (e.g. Udalski 2003).

\+ parametric expression modified to extrapolate to $\lambda > 0.9$ μm with $\lambda^{-\alpha}$.

Table 4.2: *Effective extinction, $\langle A \rangle / A_{K_S}$, using M-giant spectra (Fluks et al. 1994), for different bands defined by the ISOCAM and MSX filters (see Fig. 4.1). $A_{K_S}/A_{2.12} = 0.97$.*

Filter	$\lambda_{\rm ref}$	$\Delta\lambda$	Curve 1 (Mathis)	Curve 2	Curve 3 (Lutz)
			$(A_{9.7}/A_{2.12} = 0.54)$	$(A_{9.7}/A_{2.12} = 1.00)$	$(A_{9.7}/A_{2.12} = 1.00$ & no minimum)
	μm	μm	$\langle A \rangle / A_{K_S}$	$\langle A \rangle / A_{K_S}$	$\langle A \rangle / A_{K_S}$
LW2	6.7	3.5	0.21	0.21	0.41
LW5	6.8	0.5	0.18	0.15	0.41
LW6	7.7	1.5	0.21	0.26	0.43
LW3	14.3	6.0	0.18	0.34	0.34
LW9	14.9	2.0	0.14	0.29	0.29
A	8.28	4.0	0.26	0.38	0.55
C	12.1	2.1	0.25	0.49	0.49
D	14.6	2.4	0.14	0.29	0.29
E	21.3	6.9	0.17	0.41	0.41

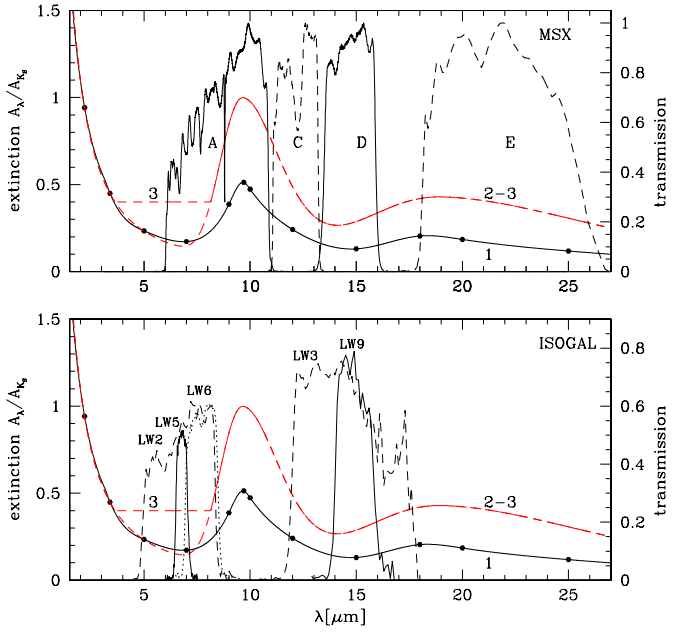

Figure 4.1: *Filter transmission curves and extinction laws as function of wavelength. The continuous line shows the curve (Curve 1) obtained by fitting the values (dots) given by Mathis (1990); the dashed curve shows the parametric expression given by Rosenthal et al. (2000) plotted using a value of the silicate peak $A_{9.7}/A_{2.12} = 1.0$ (Curve 2). The latter is also shown without the minimum around 4-8 μm (Curve 3), following Lutz (1999).* **In the top panel** *the transmission curves of the MSX A, C, D and E filters are also overplotted, while* **in the bottom panel** *the transmission curves of the ISOCAM $LW2, LW3, LW5, LW6$ and $LW9$ filters used in the ISOGAL survey are shown.*

vey. Using observations in the $LW2$ and $LW3$ bands in the inner Galactic disk they obtained $A_{\rm LW2}/A_{\rm LW3} = 0.7$, and using observations in the two bands $LW6$ and $LW9$ in the region ($|l| < 1^\circ,\ 0.2^\circ < |b| < 0.4^\circ$) they found $A_{\rm LW6}/A_{\rm LW9} = 0.8$. Both these values are in good agreement with the extinction curve calculated by Draine & Lee (1984) with a silicate peak at 9.7 μm of 1.0 (Curve 2 in Table 4.2). However, for the clouds located at ($|l| < 1^\circ, |b| < 0.2^\circ$) observed in the $LW5$ and $LW9$ bands Hennebelle et al. (2001) found $A_{\rm LW5}/A_{\rm LW9} = 1.07$, which is twice the value predicted by Curve 2 in Table 4.2, but would be consistent with Curve 1 or 3.

For stars in the inner disk Jiang et al. (2003) derived $(A_{\rm K_S} - A_{\rm LW2})/(A_{\rm J} - A_{\rm K_S}) = 0.35$ and $(A_{\rm K_S} - A_{\rm LW3})/(A_{\rm J} - A_{\rm K_S}) = 0.39$. These ratios when combined with the near-infrared extinction law imply that $A_{\rm LW2}/A_{\rm K_S}$ must range from 0.35 to 0.47 and $A_{\rm LW3}/A_{\rm K_S}$ from 0.28 to 0.41, which are higher values than those produced by Curve 1 and suggest an attenuation of the minimum at 4-8 μm, consistent with

Curve 3.

Concluding, there is some uncertainty in the mid-infrared extinction law that is in part due to uncertainties in the photometric measurements and possibly due to spatial variations in the strength of the silicate features. In the most obscured regions ($A_{\rm K_S}= 3$) uncertainties for the ISOGAL and MSX filters range from 0.45 mag ($LW3, LW9, D$) to 0.85 mag (A). However, this has a negligible effect (0.1 mag in average) on the calculated $M_{\rm bol}$ of the SiO targets because their energy is emitted mostly at near-infrared wavelengths, and has therefore also a negligible effect on the mass-loss rate estimates (see Sect. 4.5).

In the following we will use the Lutz law (Curve 3) to deredden the colours of our SiO targets, since this law ensures a consistency between mid-infrared and near-infrared stellar colours as found by Jiang et al. (2003).

4.2 Interstellar extinction of field stars from near-infrared colour-magnitude diagrams

Most of the sources detected by DENIS and 2MASS toward the inner Galaxy are red giants and asymptotic giant branch stars. Because the intrinsic $(J - K_S)_0$ colours of giants are well known and steadily increase from 0.6 to 1.5 mag with increasing luminosity, one can study the colour-magnitude diagrams (CMDs) of $(J - K_{\rm s})$ versus $K_{\rm s}$ and of $(H - K_{\rm s})$ versus $K_{\rm s}$ to estimate the average extinction toward a given line of sight for a population of such stars.

Under the assumption that our SiO targets are spatially well mixed with the red giant stars, and that the interstellar extinction is uniform over a $4' \times 4'$ field (corresponding to 9×9 pc^2 at the distance of the Galactic Centre), we estimate the extinction, $A_{\rm K_S}$, towards our 441 SiO targets by examining the CMDs of 2MASS sources in field of 2-4′ radius around each SiO target. Figure 2 shows a representative sample of these CMDs. We assume that the red giant branch (RGB) has the same intrinsic shape for all red giants in the inner Galaxy: the absolute magnitude of the tip of the RGB, $M_{\rm K_s}(tip)$, and the RGB colour-magnitude relation does not vary. This means that at a given distance, d, along the line of sight the observed RGB extends towards fainter magnitudes from the tip at magnitude $K_{\rm s}(tip) = M_{\rm K_s}(tip) + DM + A_{\rm K_s}$; here DM is the distance modulus corresponding to d and $A_{\rm K_S}$ the corresponding extinction in the $K_{\rm S}$ band. With increasing distance along a given line of sight the RGB becomes redder, due to the increase of interstellar extinction. The reddening is proportional to the extinction, $A_{\rm K_S}$, and the shift to fainter magnitudes equals $DM+A_{\rm K_S}$. In principle we could thus derive both DM and $A_{\rm K_S}$ as a function of distance by locating discrete features of the RGB. Due to small number fluctuations, it is difficult to estimate $K_{\rm s}(tip)$ and thus $DM+A_{\rm K_S}$. Some of the CMDs contain also the so-called "red clump" stars which all have the same absolute magnitude ($M_{\rm K_s} = -1.65$), so that they can be used to trace the stellar distribution and that of the dust along the line of sight. However, close to the Galactic centre the distance modulus and the extinction shift clump stars below the detection limits of DENIS and 2MASS.

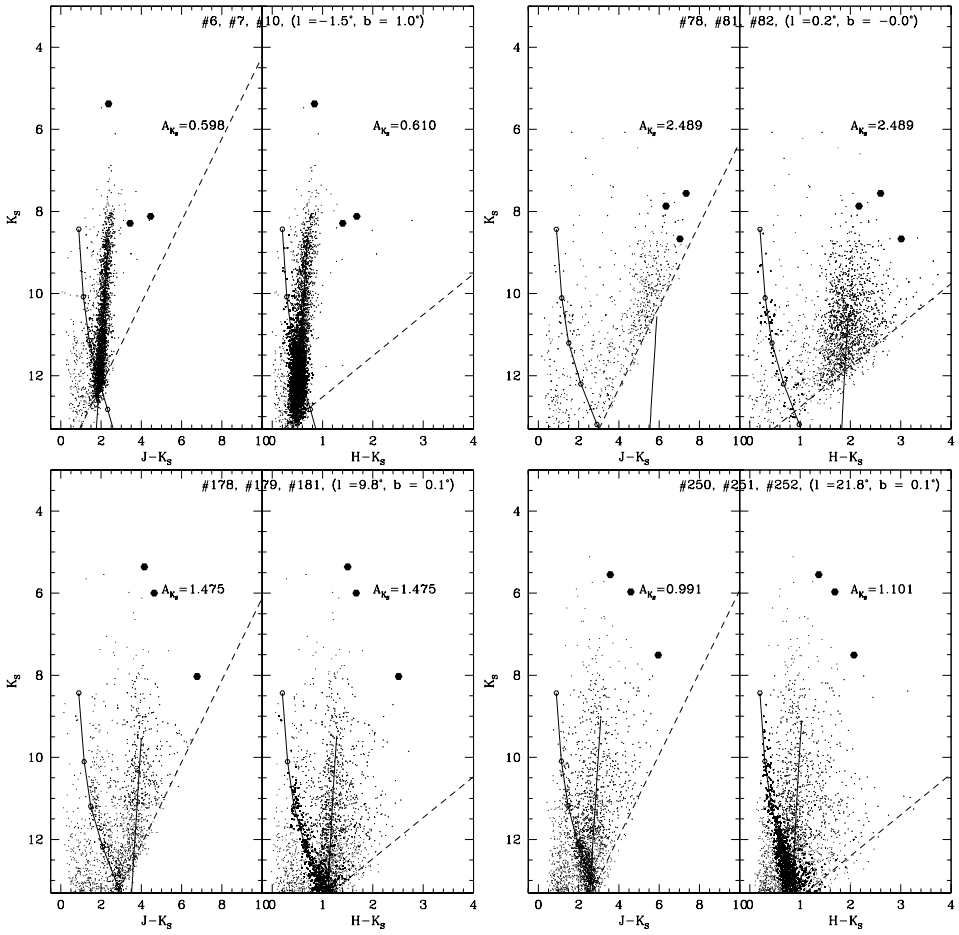

Figure 4.2: *Colour-magnitude diagrams of 2MASS datapoints (small dots) of good quality located within 4′ from the position of the SiO target (big dot). Three fields at equal median extinction are combined in each panel. The right-hand continuous line indicates the locus of the reference RGB curve (see Sect. 4.2.1), adopting a distance of 8 kpc and reddening it with the median extinction of field stars ($A_{\mathrm{K_S}}$). The left-hand continuous curve shows the trace of clump stars for increasing distance and extinction along a given line of sight (see Sect. 4.2.3), obtained using the extinction model by Drimmel et al. (2003) and the absolute magnitudes from Wainscoat et al. (1992). Dashed lines indicate the diagonal cut-offs due to the detection limits in J and H. Circles on the clump trace mark a distance from 1 to 5 kpc with a step of 1 kpc downward.*

The average field extinction can be estimated by assuming a reference isochrone (colour-magnitude relation) for the RGB (Sect. 4.2.1), and by fitting the isochrone to the observed giants. This approach was used by Schultheis et al. (1999) and Du-

tra et al. (2003) to map the extinction in the central region of the Galaxy ($|l| < 10°$). Schultheis et al. (1999) obtained an extinction map within 8° of the Galactic Centre by comparing DENIS (J, K_s) photometry with an isochrone from Bertelli et al. (1994) (metallicity $Z = 0.02$, age 10 Gyr, distance 8 kpc), adopting the extinction law of Glass (1999). A similar map was also produced by Dutra et al. (2003) using 2MASS (J, K_s) data together with an empirical reference RGB isochrone, which is a linear fit to the giants in Baade's windows, and adopting the extinction law of Mathis (1990).

The SiO targets are located at longitudes l between 0° and 30° and mostly at latitude $b < 0.5°$. In this region of high extinction even at near-infrared wavelengths, fits to the apparent (K_S, $J-K_S$) RGB may underestimate the extinction, due to observational bias as explained in Sect. 4.2.2 (see also Cotera et al. 2000; Dutra et al. 2003; Figer et al. 2004). Therefore it is useful to also consider the (K_S, $H-K_S$) plane, which is deep and not sensitive to extinction and therefore less affected by bias.

The extinction toward each of the SiO targets was calculated from individual field stars in both the (K_S, $J-K_S$) and (K_S, $H-K_S$) CMDs by shifting the datapoints on the reference RGB (see Sect. 4.2.1) along the reddening vector. Then, the median extinction of the field was determined in both the (K_S, $J-K_S$) and (K_S, $H-K_S$) planes, applying an iterative 2σ clipping to the extinction distribution in order to exclude foreground stars (Dutra et al. 2003). A comparison of the extinction estimates derived from both diagrams, and possible selection effects are described in Sect. 4.2.2.

SiO targets usually appear redder than neighbouring stars (Fig. 4.2), which implies that they are intrinsically obscured if we assume that the spatial distribution of SiO targets is the same as that of red giant branch stars. About fifty of our 441 SiO target stars are brighter in K_S and bluer than sources in the field, so those must be nearer than the median.

The CMDs contain much information on the distribution of stars and dust in the inner Galaxy. Here we have used them only to estimate a median extinction, A_{K_s}. In a future study we hope to make a more complete analysis of these diagrams with a more self-consistent model. In the following some general remarks from the analysis of the CMDs are summarised:

- We can determine A_{K_s} for individual stars in each CMD and the statistical properties of the extinction values within a given CMD. In most CMDs the interstellar extinction, A_{K_s}, shows a strong concentration, which reflects the Bulge and the Galactic centre. In a minority of CMDs the histogram is broad without clear peaks.

- Broad, diffuse extinction distributions are found at longitudes $20° < l < 30°$. This suggests that stars and dust are spread along these line of sight.

- Lines of sight which pass through complex star forming regions such as M17 are easily identified as regions of anomalously high extinction compared to their surrounding regions.

- Toward some lines of sight, especially at latitudes above $|b| \approx 0.6\ ^\circ$, a sharp edge at the high end is found in the extinction distribution. These lines of sight apparently extend to above the dust layer.

Table 4.3: *Extinction values. The identification number (ID) of the SiO target, as in Table 2 and 3 of Chapter II, is followed by the field extinction $A_{\mathrm{K_S}}$, by the corresponding dispersion of individual extinctions of field stars, and by the total extinction in K_{S}-band toward the target star (tot). Finally, a flag (Fg) is listed, which is equal to unity when the SiO target is classified as a "foreground object". Stars for which not all J, H, K_{S} measurements were available have no total extinction.*

ID	$A_{\mathrm{K_S}}$ mag	$\sigma_{A_{\mathrm{K_S}}}$ mag	tot mag	Fg	ID	$A_{\mathrm{K_S}}$ mag	$\sigma_{A_{\mathrm{K_S}}}$ mag	tot mag	Fg	ID	$A_{\mathrm{K_S}}$ mag	$\sigma_{A_{\mathrm{K_S}}}$ mag	tot mag	Fg	ID	$A_{\mathrm{K_S}}$ mag	$\sigma_{A_{\mathrm{K_S}}}$ mag	tot mag	Fg
1	0.96	0.18	1.63		61	1.72	0.29	3.46		121	1.65	0.28	1.91		181	1.38	0.59	2.77	
2	1.23	0.31	2.81		62	1.70	0.28	2.47		122	1.55	0.25	2.10		182	1.29	0.19	1.46	
3	1.90	0.33	1.79		63	2.44	0.42	3.18		123	1.26	0.36	1.51		183	1.32	0.28	1.45	
4	2.16	0.52	3.00		64	2.28	0.42	3.67		124	1.43	0.30	2.18		184	1.44	0.29	1.62	
5	1.51	0.25	1.75		65	2.28	0.42	3.67		125	1.65	0.35	2.26		185	1.37	0.24	0.44	1
6	0.59	0.09	1.16		66	1.71	0.21	1.21	1	126	0.75	0.11	1.59		186	1.57	0.18	1.51	
7	0.57	0.07	0.51		67	1.62	0.26	2.09		127	0.91	0.19	1.78		187	0.97	0.33	1.65	
8	1.98	0.41	1.53	1	68	1.68	0.23	1.09	1	128	1.51	0.24	1.60		188	0.85	0.22	1.06	
9	2.14	0.32	2.59		69	2.17	0.43	2.53		129	0.93	0.24	0.36	1	189	0.21	0.04	1.14	
10	0.61	0.11	1.48		70	1.65	0.36	2.02		130	0.79	0.09	0.52	1	190	1.04	0.59	1.10	
11	0.94	0.17	1.04		71	1.84	0.35	2.12		131	1.69	0.44	1.94		191	2.22	0.75	3.39	
12	1.21	0.17	1.61		72	1.86	0.23	2.24		132	1.61	0.42	2.53		192	0.93	0.33	1.69	
13	1.11	0.23	2.15		73	2.63	0.30	3.94		133	0.99	0.19	0.86		193	0.97	0.34	1.60	
14	1.38	0.14	1.66		74	1.42	0.18	1.92		134	1.52	0.26	2.60		194	1.37	0.20	1.94	
15	1.34	0.27	0.89	1	75	1.36	0.23	1.19		135	1.20	0.27	1.46		195	1.42	0.14	1.71	
16	1.46	0.15	1.99		76	2.71	0.38	3.58		136	1.27	0.13	1.48		196	1.85	0.79	2.84	
17	1.45	0.15	1.86		77	2.49	0.43	2.22		137	1.21	0.24	1.73		197	1.91	0.53	2.02	
18	1.53	0.27	1.89		78	2.49	0.43	3.74		138	1.11	0.19	2.17		198	1.76	0.47	2.46	
19	0.60	0.06	0.71		79	1.88	0.34	1.93		139	0.21	0.04	0.95		199	1.22	0.31	0.57	1
20	1.47	0.21	1.81		80	2.12	0.28	2.81		140	1.03	0.13	0.38	1	200	2.10	1.07	1.97	
21	1.40	0.29	1.35		81	2.53	0.38	2.56		141	1.22	0.17	2.49		201	0.92	0.24	1.49	
22	1.40	0.29	1.82		82	2.45	0.40	3.33		142	1.22	0.16	1.26		202	0.92	0.24	0.14	1
23	1.73	0.63	1.06	1	83	1.58	0.23	1.50		143	1.30	0.19	1.96		203	0.91	0.26	3.15	
24	2.17	0.36	3.07		84	2.34	0.39	2.90		144	1.49	0.32	1.36		204	0.97	0.25	3.04	
25	1.83	0.26	1.10	1	85	2.24	0.44	2.25		145	1.02	0.18	0.98		205	1.19	0.32	1.46	
26	2.26	0.40	2.73		86	2.21	0.68	2.88		146	0.83	0.15	1.06		206	2.36	0.48	0.45	1
27	1.93	0.24	2.19		87	1.69	0.14	1.24	1	147	1.34	0.27	0.89	1	207	1.15	0.29	1.17	
28	2.09	0.36	2.77		88	2.45	0.51	3.07		148	0.80	0.21	0.57	1	208	0.91	0.33	1.41	
29	2.56	0.32	4.31		89	2.60	0.41	2.97		149	1.17	0.25	1.43		209	1.91	0.63	2.70	
30	2.82	0.36	3.92		90	1.90	0.34	2.12		150	1.33	0.31	2.23		210	0.88	0.24	1.64	
31	1.80	0.19	1.72		91	2.82	0.52	3.09		151	1.17	0.32	1.41		211	1.42	0.53	2.50	
32	1.61	0.24	1.78		92	1.66	0.28	1.40		152	1.08	0.39	1.88		212	0.82	0.31	2.02	
33	1.62	0.22	2.69		93	1.87	0.35	1.85		153	0.14	0.15	0.34		213	2.56	1.05	4.03	
34	1.78	0.25	2.67		94	2.07	0.47	3.62		154	1.73	0.64	5.16		214	1.00	0.19	1.13	
35	1.89	0.23	2.50		95	2.11	0.76	4.65		155	1.20	0.30	1.55		215	1.30	0.36	3.56	
36	1.47	0.22	0.80	1	96	1.92	0.32	1.88		156	0.97	0.25	1.75		216	0.89	0.35	1.43	
37	1.87	0.25	3.37		97	2.31	0.61	3.38		157	1.31	0.33	1.42		217	1.02	0.34	1.89	
38	2.98	0.44	3.52		98	2.37	0.61	2.94		158	1.42	0.32	1.60		218	1.30	0.65	1.40	
39	2.91	0.44	3.64		99	2.41	0.56	2.34		159	1.46	0.19	2.15		219	1.48	0.31	2.15	
40	2.29	0.35	2.79		100	2.30	0.56	3.55		160	1.35	0.23	0.81	1	220	2.21	0.57	3.39	
41	2.68	0.40	3.53		101	2.11	0.39	3.89		161	1.84	0.35	2.12		221	1.10	0.35	2.24	
42	2.19	0.41	2.37		102	2.24	0.48	2.24		162	1.66	0.41	3.35		222	1.93	0.37	2.29	
43	1.66	0.26	3.29		103	0.99	0.16			163	1.75	0.47	2.25		223	1.02	0.29	1.87	
44	1.75	0.21	1.86		104	0.92	0.10	1.21		164	1.32	0.30	1.49		224	2.04	0.57		
45	2.67	0.34	3.76		105	1.62	0.31	2.32		165	1.08	0.21	2.67		225	1.53	0.48	2.24	
46	2.89	0.47	4.44		106	1.23	0.54	2.10		166	1.21	0.26	2.44		226	0.84	0.28	1.10	
47	1.34	0.11	1.15	1	107	1.70	0.42	2.56		167	1.26	0.18	1.58		227	1.83	0.26	0.61	1
48	2.25	0.39	2.67		108	2.01	0.56	0.77	1	168	1.35	0.16	1.52		228	0.92	0.32	1.94	
49	2.33	0.41	2.69		109	1.88	0.39	2.98		169	1.11	0.48	1.98		229	1.32	0.43	2.29	
50	1.10	0.16	1.75		110	1.78	0.53	2.64		170	1.19	0.19	1.96		230	0.87	0.26	1.61	
51	2.31	0.39	3.70		111	1.81	0.38	2.10		171	1.57	0.31	1.67		231	0.70	0.22	1.54	
52	2.33	0.38	3.86		112	1.35	0.30	1.32		172	1.09	0.33	2.79		232	1.10	0.35	1.45	
53	2.68	0.34	2.65		113	1.70	0.28	1.14	1	173	1.61	0.63	1.20		233	1.64	0.54	1.56	
54	2.31	0.38	2.33		114	1.25	0.28	1.47		174	1.02	0.53	1.49		234	1.18	0.38	2.17	
55	1.71	0.27	2.94		115	1.92	0.43	2.00		175	1.20	0.39	2.09		235	1.00	0.36	1.77	
56	2.34	0.36	2.49		116	1.75	0.46	1.41		176	1.42	0.50	1.46		236	0.81	0.30	1.90	
57	2.55	0.45	3.49		117	1.85	0.41	3.25		177	1.27	0.30	1.51		237	0.75	0.23	2.00	
58	2.20	0.33	3.59		118	2.78	0.59	3.97		178	1.50	0.37	1.48		238	0.95	0.37	1.34	
59	2.25	0.34	2.38		119	1.63	0.60	1.54		179	1.43	0.32	1.79		239	0.83	0.30	1.49	
60	2.11	0.29	2.75		120	1.62	0.29	2.27		180	1.20	0.38	1.05		240	0.76	0.30	2.00	

Table 4.3: *(continued)*

ID	A_{K_S} mag	$\sigma_{A_{K_S}}$ mag	tot mag	Fg	ID	A_{K_S} mag	$\sigma_{A_{K_S}}$ mag	tot mag	Fg	ID	A_{K_S} mag	$\sigma_{A_{K_S}}$ mag	tot mag	Fg	ID	A_{K_S} mag	$\sigma_{A_{K_S}}$ mag	tot mag	Fg
241	0.92	0.29	2.05		301	2.13	0.33	1.88		361	1.60	0.49	3.67		421	1.06	0.45	3.64	
242	0.88	0.20	0.93		302	2.56	0.33	2.50		362	1.35	0.18			422	1.25	0.44	1.86	
243	0.92	0.32	2.42		303	1.36	0.11	0.63	1	363	1.87	0.41	3.00		423	0.72	0.68	0.32	
244	0.96	0.39	0.99		304	2.07	0.35	3.41		364	0.61	0.09	0.96		424	1.34	0.40	2.28	
245	0.67	0.22	0.89		305	1.79	0.22	2.53		365	1.72	0.26	3.62		425	1.72	0.71	1.37	
246	1.15	0.44	1.65		306	1.88	0.24	2.06		366	0.60	0.15	1.21		426	1.07	0.47	2.53	
247	1.26	0.36	0.79	1	307	1.24	0.13	1.48		367	1.16	0.32	2.95		427	0.90	0.46		
248	1.26	0.39	1.61		308	2.20	0.36	2.92		368	1.57	0.31	0.63	1	428	0.94	0.41	1.53	
249	0.98	0.42	2.31		309	2.26	0.35	2.52		369	1.35	0.22	2.58		429	0.74	0.39	1.70	
250	0.93	0.42	2.36		310	2.79	0.41	2.42		370	1.11	0.23	0.53	1	430	0.88	0.32	1.63	
251	1.39	0.42	1.74		311	2.93	0.51	4.32		371	0.83	0.14	1.49		431	0.83	0.31	1.17	
252	0.92	0.31	1.23		312	1.70	0.28	2.14		372	1.24	0.16	2.13		432	0.97	0.35	1.17	
253	0.96	0.32	2.34		313	1.75	0.28	2.25		373	1.24	0.11	1.12	1	433	0.72	0.29	1.84	
254	1.27	0.55	1.82		314	2.18	0.46	3.18		374	0.95	0.20	1.36		434	1.71	0.60	1.84	
255	1.13	0.30	1.22		315	1.05	0.13	1.47		375	1.03	0.21	1.70		435	1.02	0.45	0.40	1
256	0.84	0.61	2.80		316	1.54	0.22	1.77		376	1.33	0.22	2.97		436	0.97	0.36	0.00	1
257	0.90	0.38	4.34		317	1.32	0.15	1.53		377	1.11	0.22	1.80		437	1.01	0.34	3.31	
258	1.64	0.70	2.88		318	1.63	0.25	2.15		378	0.80	0.24	1.00		438	0.99	0.30	0.38	1
259	0.85	0.48	1.07		319	0.61	0.08	1.16		379	0.84	0.19	0.68		439	0.99	0.34	2.42	
260	1.08	0.43	1.67		320	2.20	0.33	2.60		380	1.03	0.31	2.52		440	1.03	0.32	0.45	1
261	1.62	0.37	2.44		321	2.28	0.43			381	1.79	0.55	2.60		441	1.02	0.44	1.34	
262	1.45	0.34	1.71		322	2.23	0.41	3.79		382	0.86	0.16	0.95		442	1.17	0.53	2.69	
263	0.91	0.49	1.80		323	1.87	0.25	2.92		383	1.13	0.31	1.52		443	0.96	0.57		
264	1.11	0.36	1.78		324	2.41	0.49	3.49		384	1.33	0.35	0.86	1	444	1.16	0.70	0.88	
265	0.84	0.33	1.48		325	2.13	0.43	2.08		385	1.17	0.39	1.67						
266	0.75	0.30	1.52		326	1.74	0.21	2.62		386	1.61	0.20	1.23	1					
267	0.72	0.34	1.04		327	2.17	0.25	3.09		387	2.00	0.55	5.02						
268	0.74	0.30	2.59		328	1.39	0.21	1.95		388	1.77	0.56	3.17						
269	0.82	0.30	1.32		329	1.74	0.24	2.06		389	1.28	0.23	2.15						
270	0.88	0.31	2.22		330	1.90	0.28	2.59		390	1.56	0.32	1.36						
271	1.00	0.54	2.46		331	2.15	0.27	3.22		391	1.58	0.31	2.36						
272	1.48	0.30	1.51		332	2.58	0.37	2.89		392	1.39	0.29	2.19						
273	1.80	0.45			333	2.41	0.44	3.12		393	0.75	0.19	1.39						
274	0.49	0.05	0.96		334	2.59	0.45	2.27		394	1.16	0.46	2.31						
275	0.47	0.05	0.40	1	335	2.33	0.52	2.13		395	0.92	0.22	0.63	1					
276	2.27	0.60	3.76		336	2.14	0.23	2.82		396	1.24	0.26	0.37	1					
277	0.57	0.07	0.49	1	337	1.37	0.15	1.52		397	1.03	0.29	1.04						
278	2.12	0.40	2.92		338	2.23	0.34	2.23		398	1.55	0.29	0.38	1					
279	0.98	0.17	1.23		339	2.28	0.33	2.28		399	1.08	0.29	1.45						
280	1.18	0.21	1.60		340	1.26	0.19	1.50		400	1.39	0.34	4.32						
281	0.93	0.14	1.34		341	2.83	0.58	4.58		401	1.24	0.21	1.34						
282	1.38	0.19	2.09		342	2.62	0.39	3.31		402	1.79	0.27	0.00	1					
283	1.21	0.11	1.51		343	2.60	0.52	2.56		403	1.89	0.51							
284	0.83	0.12	1.54		344	2.69	0.50	2.47		404	3.43	0.48	3.90						
285	1.15	0.14	1.50		345	2.13	0.61	2.61		405	2.49	1.05	0.80	1					
286	0.61	0.06	0.32	1	346	2.51	0.56	2.90		406	1.56	0.21	2.01						
287	0.55	0.06	0.41	1	347	2.89	0.62	0.63	1	407	0.54	0.19	2.59						
288	1.43	0.21	2.15		348	2.04	0.35	3.73		408	1.41	0.16	3.58						
289	1.72	0.31	2.06		349	1.63	0.27	3.79		409	1.00	0.35	2.43						
290	1.51	0.22	1.70		350	1.85	0.41	1.94		410	1.27	0.38	1.85						
291	1.41	0.14	0.96	1	351	1.38	0.28	2.73		411	1.02	0.34	3.10						
292	1.63	0.21	2.07		352	1.25	0.24	1.69		412	1.77	0.46	1.76						
293	1.62	0.30	2.21		353	1.71	0.26	2.28		413	2.13	0.44	3.65						
294	2.23	0.50	2.37		354	1.36	0.25	2.63		414	0.78	0.25	1.57						
295	1.67	0.22	2.18		355	1.55	0.23	2.17		415	0.95	0.25							
296	1.54	0.18	1.54		356	0.82	0.11	1.08		416	0.73	0.27	0.64						
297	2.35	0.28	1.07	1	357	1.84	0.46	3.40		417	0.93	0.27							
298	1.50	0.17			358	1.64	0.31	0.96	1	418	0.94	0.34	3.61						
299	1.54	0.15	1.99		359	1.38	0.27	2.26		419	0.79	0.37	3.41						
300	2.28	0.32	3.73		360	1.46	0.29	1.36		420	1.16	0.39	3.27						

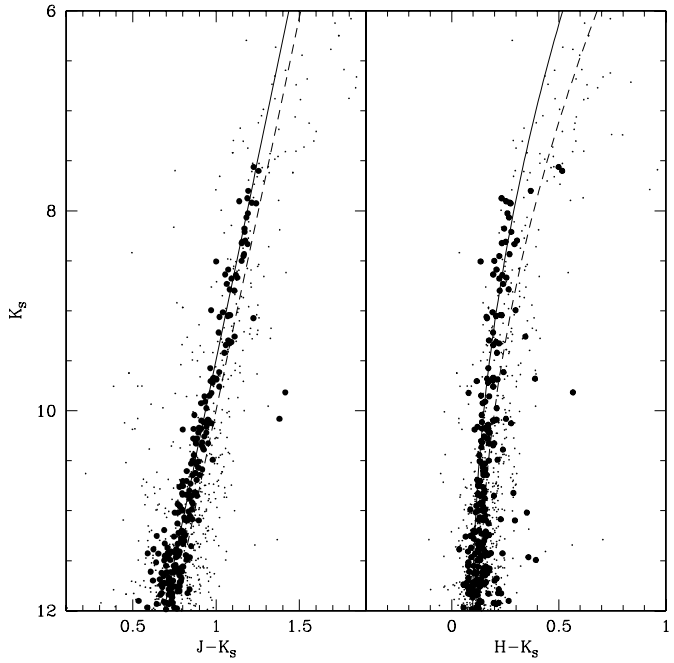

Figure 4.3: *Magnitudes versus colours of 2MASS stars. Large dots are 2MASS sources within 4′ from the centre of the globular cluster 47 Tuc, brought at the distance of 8 kpc adopting a distance modulus of 13.32 (Ferraro et al. 1999). Small dots are dereddened 2MASS Sgr–I field sources, selected within 30″ from Mira stars (Glass et al. 1995) in order to overpopulate the Mira region above the RGB tip. Continuous lines indicate the mean ridge lines for the cluster red giant branch, while dashed lines those of the Sgr–I giants.*

4.2.1 Reference red giant branch

In Figure 4.3 we plot the extinction-corrected 2MASS point sources within 30″ from the positions of Mira stars in the Sgr–I field (Glass et al. 1995). Objects above the RGB tip ($K_{\rm S}\sim 8.2$ mag) are AGB stars: 63 Mira variables from (Glass et al. 1995) and 24 other stars, most probably semiregular (SR) variables (Alard et al. 2001). In the same diagram we also plot 2MASS sources within 4′ from the centre of the Galactic globular cluster 47 Tuc, moved to a distance of 8 kpc (cluster distance modulus, DM=13.32 mag, from Ferraro et al. 1999).

The upper part ($K_{\rm S}< 12$ mag) of the 47 Tuc RGB in the $K_{\rm S0}, (J-K_{\rm s})_0$ CMD is well represented by a linear fit:

$$(\mathrm{J-K_s})_0 = 2.19(\pm0.02) - 0.125(\pm0.002)\mathrm{K_{S0}}. \quad (4.1)$$

The 47 Tuc giants appear bluer by 0.05 mag in $(J - K_{\rm s})_0$ than the colours of Sgr–I giants, which are more metal rich. However, the cluster $(J - K_{\rm s})_0$ vs. K_{S0} RGB has a slope identical to that found in Sgr–I, confirming that the slope does not vary significantly with metallicity (see Dutra et al. 2003; Frogel et al. 1999).

To assess the uncertainty of our extinction estimates, we examined the model RGB colours of Girardi et al. (2000) with two extreme values of metallicity, Z=0.04 and 0.30. These models do not show a significant difference in the CMD slope, and they differ in $(J-K_{\rm s})_0$ by only 0.1 mag. A similarly small difference is found for models of 2 Gyr and 16 Gyr old populations. Nominal 2MASS photometric errors are smaller than 0.04 mag for $J < 15$ and $K_{\rm S}< 13$ mag, but toward the Galactic centre uncertainties are larger because of crowding. However, all the uncertainties have a small impact on the extinction estimates: a change of 0.1 in $(J - K_{\rm s})_0$ implies a change of 0.05 in $A_{\rm K_s}$ (0.6 in $A_{\rm V}$).

The right-hand panel of Fig. 4.3 shows the $(H - K_{\rm s})_0$ vs. K_{S0} diagram of Sgr–I giants and of the 47 Tuc giants. There is again a well defined RGB sequence. A second order polynomial fit well fits 47 Tuc giants with $K_{\rm S0} < 12$ mag:

$$(\mathrm{H} - \mathrm{K_s})_0 = 1.73(\pm 0.22) - 0.268(\pm 0.035) \times \mathrm{K_{S0}} \qquad (4.2)$$

$$+0.011(\pm 0.002) \times \mathrm{K_{S0}^2}.$$

At $K_{\rm S0} < 8$ mag this fit traces the blue boundary toward Mira stars. A fit of only Sgr–I giants is slightly more shallow:

$$(\mathrm{H} - \mathrm{K_s})_0 = 2.25(\pm 0.13) - 0.347(\pm 0.029) \times \mathrm{K_{S0}} \qquad (4.3)$$

$$+0.014(\pm 0.002) \times \mathrm{K_{S0}^2}.$$

The $K_{\rm s}, (H-K_{\rm s})$ plane has a lower sensitivity to extinction than the $K_{\rm s}, (J-K_{\rm s})$ plane: here a colour change of 0.1 mag implies a change of ~ 0.15 in $A_{\rm K_s}$. The models of Girardi et al. (2000) predict variations within $(H - K_{\rm s}) = 0.04$ mag with metallicity and age variations. The nominal 2MASS photometric errors are smaller than 0.04 for $H < 14$ and $K_{\rm S}< 13$.

The uncertainty in distance yields only a minor uncertainty in the extinction. A shift in distance modulus of the reference RGB of ± 2 mag results in a change in the extinction of $A_{\rm K_s} \mp 0.15$ mag.

4.2.2 Determination of extinction value and extinction law in the J, H, $K_{\rm s}$ CMD

Assuming a colour-magnitude relation for red giants, the apparent near-infrared colours of field stars yield information on, both, the magnitude of the extinction and on the shape of the extinction law.

In principle, one can try to fit the observed field star colours to the red giant branch colours in the near-infrared colour-magnitude diagrams, and optimise the fit for both the absolute average extinction in the $K_{\rm s}$ band along the line of

sight and the spectral index of the extinction power law. To do that, one needs to consider only the region of the colour-magnitude diagram where the upper RGB is well defined, i.e. not affected by large photometric errors or by the diagonal cut-off from the 2MASS detection limits (see Fig. 4.2), which would bias the calculation of the median extinction toward a lower value. In the inner Galaxy, the photometric error is typically below 0.04 for stars with $K_{\rm s} < 12$ mag. To quantify the incompleteness due to the diagonal cut-off, with zero extinction, our average 2MASS detection limits of $J = 16.0$ and $H = 14.0$ correspond to a RGB $K_{\rm S}$ magnitude of 15.2 and 13.0 mag, respectively, at a distance of 8 kpc. Accounting for a scatter in the observed colours of ± 0.5 mag, the RGB would be sampled well to $J = 15.5$ and $H = 13.5$ mag, corresponding to $K_{\rm S} < 14.6$ and 12.6, respectively. With a $K_{\rm S}$ extinction of 3 mag (~ 5.0 mag in H, ~ 8.6 mag in J), a typical value in the direction of the Galactic centre, these RGB completeness limits would rise to $K_{\rm s} = 7.1$ and 10.8 mag in the $(K_{\rm s}, J - K_{\rm s})$ and $(K_{\rm s}, H - K_{\rm S})$ planes, respectively. In the J band we would therefore be left with variable AGB stars well above the RGB tip and foreground stars, and only the H band would provide a sufficient number of red giant stars to match the reference RGB. We conclude from this that with the 2MASS data $(K_{\rm s}, J - K_{\rm s})$ colour-magnitude diagrams are useful for extinction determinations only to a $K_{\rm S}$ extinction of about 1.6 mag, and one must always make sure that only stars above the completeness limit are matched to the RGB. Because of the larger reddening, the $(K_{\rm s}, J - K_{\rm s})$ plane would in principle give more accurate extinction estimates, would it not be affected by the selection effect due to the relatively bright detection limit.

To determine the slope, α, of the near-infrared extinction law we examined the CMDs for field stars which were detected in all three bands, J, H, and $K_{\rm S}$, brighter than the $K_{\rm S}$ completeness limits for the RGB at the extinction of each field. We determined the extinction toward each of our fields separately in the $(K_{\rm S}, J - K_{\rm s})$ and $(K_{\rm s}, H - K_{\rm s})$ CMDs, as the median of the extinctions from individual field stars. The difference of the extinction determinations from the two planes must agree independent from $A_{\rm K_S}$ within the dispersion.

Therefore, we vary α until we get an overall agreement between the extinction estimates from the two planes. Figure 4.4 shows the differences of the median extinction values $A_{\rm K_S}(J,K_{\rm S}) - A_{\rm K_S}(H,K_{\rm S})$ plotted against the $A_{\rm K_S}$ -calculated- for different values of α. The discrepancy between the extinction values increases with $A_{\rm K_S}$ if the assumed value of α is too small. We find that for $\alpha = 1.9$ the two extinction estimates do yield consistent values, within the photometric uncertainties, over the entire range of $A_{\rm K_S}$.

The main uncertainty in the determination of the extinction power law arises from the uncertainty in the slope of the RGB. Using a fit to the colour-magnitude distribution of the giants in the Sgr–I field ($l = 1.4°$,b$= -2.6$) instead of the 47 Tuc globular cluster giants, that is somewhat steeper in the ($K_{\rm S}$,$H-K_{\rm S}$) plane, we find that the best value for alpha increases to 2.2.

The slope of the RGB decreases with increasing metallicity, leading to higher values of α. However, since 47 Tuc has a lower metallicity (-0.7 dex) than the average Bulge stars (Frogel et al. 1999; McWilliam & Rich 1994), $\alpha = 1.9$ may be

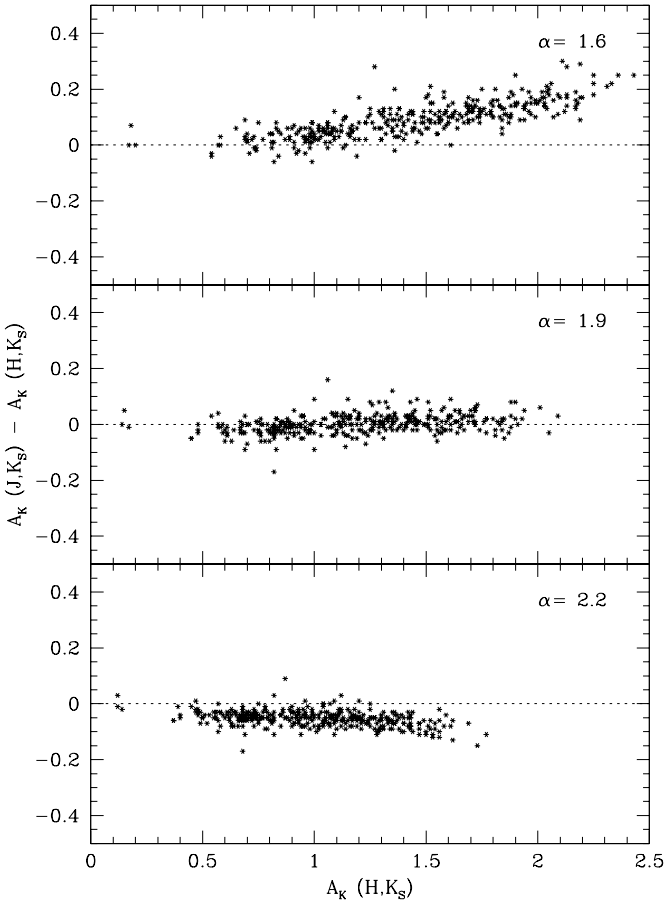

Figure 4.4: *Comparison between the median extinction values toward our fields obtained from the (K_S,$J-K_S$) plane and those from the (K_S,$H-K_S$) plane. Only sources detected in J, H,K_S above the K_S completeness limits are used. In each panel a different value of the spectral index of the extinction power law, α, is adopted.*

taken as a lower limit to the actual value.

We furthermore find that the (K_S,$H-K_S$) distribution of the giants in the low extinction region (A_{K_S}=0.2) at $l = 0.2°$and b= -2.1 (Dutra et al. 2002; Stanek 1998) match the distribution of the 47 Tuc giants better than that of Sgr–I.

Although complicated by the intrinsic colour-magnitude relation that giant stars follow, the value of the α parameter can be tested using a $J - H$ vs. $H-K_S$ diagram. Using the values from Table 4.1 for power laws with $\alpha = 1.6$, 1.85, 1.9, 2.0, 2.2, the slopes of the reddening vector in the $J - H$ vs. $H-K_S$ diagram are 1.64, 1.75, 1.80, 1.83, 1.94, respectively. Identical slopes are found when red-

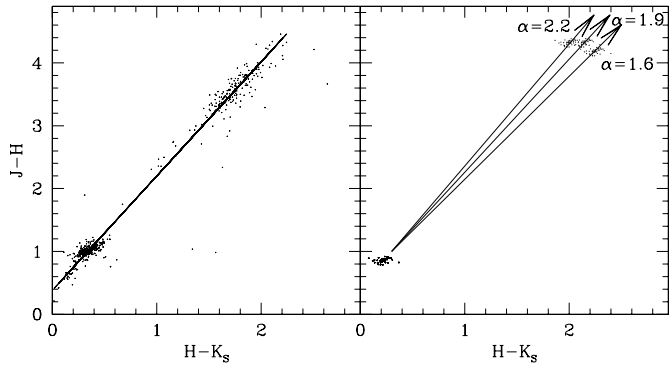

Figure 4.5: *$J-H$ vs. $H-K_{\rm S}$ colours. The arrows are the reddening vectors for a visual extinction of 35 mag and a near-infrared power law slopes α of 1.6, 1.9 and 2.0.* **Left-hand panel:** *Bulge giant stars with $10 < K_{\rm s} < 8$ mag taken from several Bulge fields at different median extinction.* **Right-hand panel:** *Giant stars from 47 Tuc with $10 < K_{\rm s} < 8$ mag when brought at the distance of the Galactic centre. The same stars are plotted again reddened using the near-infrared power laws with slope $\alpha = 1.6$, 1.9 and 2.2 and $A_{\rm K}$=2.9.*

dening artificially the 47 Tuc giants (or the Sgr–I giants) and linearly fitting the non-reddened giants plus the reddened ones. A $J-H$ vs. $H-K_{\rm S}$ diagram of giant stars from fields with median extinction between $A_{\rm K_S}= 2.0$ and 2.3 mag and from Sgr–I field is shown in Fig. 4.5. The best fit to the datapoints gives a slope of 1.81 ± 0.03, also suggesting that $\alpha = 1.9 \pm 0.1$.

The value $\alpha = 1.9$ is in agreement with the work of Glass (1999) and Landini et al. (1984) and the historical Curve 15 of van de Hulst (1946).

In the rest of the paper we use the extinction calculated assuming $\alpha = 1.9$. For fields with $A_{\rm K_S}< 1.6$ mag we adopt the extinction values determined from the ($K_{\rm S}$,$J-K_{\rm S}$) plane, otherwise we will use the values from the ($K_{\rm S}$,$H-K_{\rm S}$) plane.

4.2.3 Outside the Bulge

K2 giant stars are the dominant population of late-type stars seen along the disk (e.g. Drimmel et al. 2003; López-Corredoira et al. 2002). They correspond to red clump stars in metal-rich globular clusters such as 47 Tuc. The location of clump stars on the CMD depends on extinction and distance. This trace was modelled taking the absolute magnitudes of clump stars from Wainscoat et al. (1992) and the distribution of dust and stars in the Galaxy found by Drimmel et al. (2003). The trace of the clump stars is shown by the left curve in Fig. 4.2, and it appears more populated by stars and distinct from the Bulge RGB in the CMD of the field at $l =\sim 10^\circ$.

Toward the Bulge the Bulge RGB population is dominant and therefore the

median interstellar extinction is practically not affected by possible foreground clump stars. This is not the case in the disk, where one must eliminate the foreground clump stars before fitting the RGB in order to properly calculate the median extinction of field giants.

We therefore identified as likely clump stars those located within 0.3 mag from the $J-K_{\rm S}$ colour of the clump trace, and we identify as giants those stars redder than the clump stars (e.g. López-Corredoira et al. 2002).

4.2.4 Dispersion of the extinctions along a line of sight

Toward a given target star together with the median extinction of field stars $A_{\rm K_S}$ we determined the standard deviation of the distribution of the individual extinctions, $\sigma_{\rm A_{K_S}}$.

The patchy nature of the extinction is visible even within the $2-4'$ radius sampling area. This patchiness integrated over a longer path generates larger $\sigma_{\rm A_{K_S}}$ with increasing extinction for Bulge line of sights. The $1\sigma_{\rm A_{K_S}}$ uncertainty in the field extinction varies from ~ 0.2 mag when $A_{\rm K_S}= 0.6$ mag up to ~ 0.7 mag in the regions with the largest extinction ($A_{\rm K_S}> 2.0$). In fields at longitudes longer that 10° a larger $\sigma_{\rm A_{K_S}}$ is found than in Bulge fields of similar median extinction. This is probably due to the presence of several Galactic components, e.g. the disk, arms, bar and molecular ring, along these line of sights.

4.3 Near-infrared properties of known Mira stars

As indicated by their variability, their strong 15 μm emission (Chapter III), and their SiO maser emission (Chapter II), our SiO targets are AGB stars in the thermal pulsing phase. At the present time their pulsation periods and amplitudes are not known. However, most of our SiO targets must be large amplitude variables (Chapter III).

Though they are 20 times less numerous than semiregular AGB stars (SRs) (Alard et al. 2001), Mira stars are among the best studied pulsating variable stars. They are regular long period variables (LPV) with visual light amplitude over 2.5 mag, or K band amplitude over ~ 0.3 mag. Since large amplitudes tend to be associated with the most regular light curves (Cioni et al. 2003), the amplitude remains the main parameter for the classification of a Mira star.

To analyse the colours of our SiO targets, in particular to check the quality of the extinction corrections, it is useful to have a comparison sample of large amplitude LPV AGB stars, well studied and covering a wide range of colours.

Therefore, we examined various comparison samples of known Mira stars free of extinction: two samples in the solar vicinity, taken from Olivier et al. (2001) and Whitelock et al. (2000), plus one sample toward the Galactic Cap taken from Whitelock et al. (1994). To account for possible changes in the colour properties of the Mira stars with Galactic position, we also looked at two samples of Bulge Mira stars from regions of low extinction: 18 Mira stars detected by IRAS (Glass

et al. 1995) in the Sgr–I field, and 104 IRAS Mira stars at latitude $6^\circ < b < 7^\circ$ and $|l| < 15^\circ$ (Whitelock et al. 1991); for comparison a sample of LPV in the Large Magellanic Cloud is also considered (Whitelock et al. 2003). All these stars have IRAS 12 μm magnitude, [12], and mean J, H, K magnitudes in the SAAO system (Carter 1990).

The stellar fluxes are given already corrected for reddening only in the work of Olivier et al. (2001). For the LPV stars analysed by Whitelock et al. (2000, 1994, 2003) the effects of interstellar extinction are negligible because these stars are nearby or outside of the Galactic plane and we therefore did not correct these for extinction. We dereddened the Baade Sgr–I window data (Glass et al. 1995) adopting our favourite extinction curve ($\alpha = 1.9$) and $A_{\rm K_S} = 0.15$ mag (consistently with the extinction value adopted in Glass et al. 1995). We corrected for reddening the magnitudes of the outer Bulge Miras (Whitelock et al. 1991) adopting values of $A_{\rm K_S}$ derived from their surrounding stars (see next section).

Next we analyse the location of these well-known Mira stars in the near-infrared CMDs and colour-colour diagrams.

4.3.1 Colour-magnitude diagram of outer Bulge Mira stars and surrounding field stars

Long period variable stars in the outer Bulge as studied by Whitelock et al. (1991) are interesting in several aspects: they were selected on the basis of their IRAS fluxes and colours according to criteria similar to those with which we selected our MSX targets (Chapter II; Chapter III); since their main period ranges from 170 to 722 days and their K amplitudes from 0.4 to 2.7 mag, they are classical Mira stars; their distances were estimated from the period-luminosity relation (Whitelock et al. 1991), resulting in a distribution of the distance moduli peaking at 14.7 mag with a $\sigma =\sim 0.5$ mag; since they are at latitudes between 6 and 7°, they are in regions of low interstellar extinction. All this makes them ideal objects for a comparison with our SiO targets, the study of which is complicated by the large interstellar extinction at their low latitudes.

Fig. 4.6 shows the 2MASS point sources within 1′ of each Mira star. A giant branch is clearly apparent. From an isochrone fitting (see Sect. 4.2) we derived the median extinction toward each field, resulting in values of $A_{\rm K_S}$ ranging from 0.01 to 0.30 mag, with a typical dispersion of 0.01-0.08 mag. On the colour-magnitude diagrams the Mira stars appear mostly brighter than the RGB tip of the field stars ($K = 8.2$ mag at a distance of 8 kpc, see Frogel & Whitford 1987). Due to the presence of a circumstellar envelope, Mira stars have red colours (up to $(H - K_{\rm s})_0 = 3$ mag) and lie on the red-side of the giant sequence.

It is therefore not possible to derive the interstellar extinction toward these Mira stars from their colours relative to the RGB. On the other hand, we do not have reasons to assume that the Mira stars are spatially distributed differently than the other giants stars. Therefore, the extinction of its surrounding field stars may serve as an approximation for that of the respective Mira star.

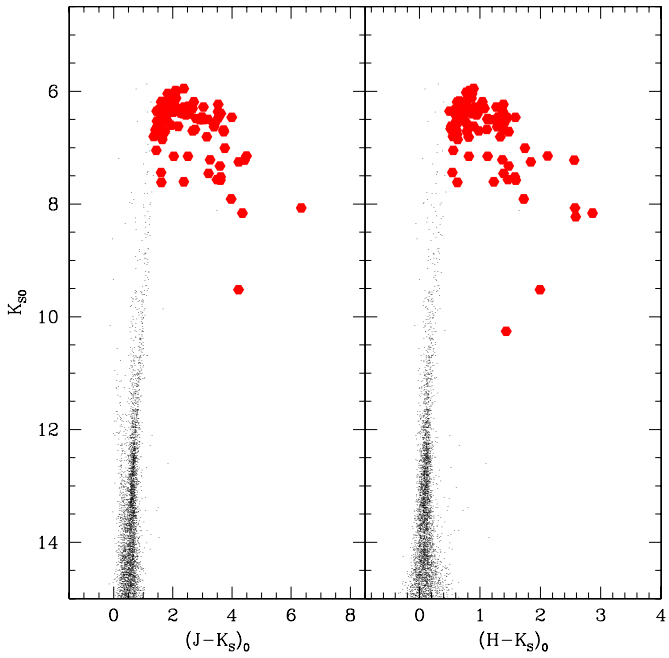

Figure 4.6: *Dereddened colour-magnitude diagrams. Big dots represent the outer Bulge Mira stars found by Whitelock et al. (1991); the magnitudes plotted are mean magnitudes at the equal distance of 8 kpc, adopting the distances of Whitelock et al. (1991). Small dots represent the point sources detected by 2MASS within 1′ from each Mira star.*

When going to lower latitude fields, however, the extinction increases and the RGB becomes broader. A worry in the assumption that a Mira star is at the median extinction of the field is the lack of knowledge of the actual distribution of extinction along the line of sight which does not warrant that the extinction of a given Mira star is the median extinction of field stars.

4.3.2 Colour-colour diagram of Mira stars

The $(J-K)_0$ vs. $(H-K)_0$ colours of Mira stars are shown in Fig. 4.7. For stars with low mass-loss rate ($< 10^{-7}$ $M_\odot$ yr^{-1}) $(J-K)_0$ ranges between 1.2 and 1.6 (Whitelock et al. 2000). Dust-enshrouded IRAS AGB stars with mass-loss rates of $10^{-6}-10^{-4}$ $M_\odot$ yr^{-1} (Olivier et al. 2001) are much redder, $(J-K)_0$ ranging from 2 to 6.5 mag. The overall distribution appears to form a sequence of ever redder colours with increasing mass-loss rate, a trend that is well reproduced, e.g., by a model for an M10 type AGB star with increasing shell opacity (Groenewegen & de Jong 1993). Thus, a higher mass loss has the same effect on $(J-K)_0$ and $(H-K)_0$ colours as more interstellar absorption/reddening, making a distinction

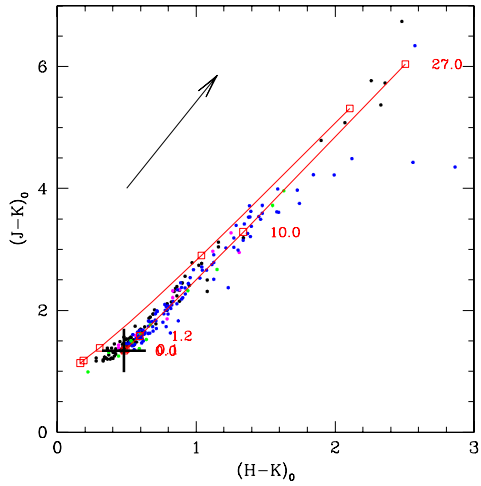

Figure 4.7: *Dereddened colours of known dusty Mira stars (Glass et al. 1995; Olivier et al. 2001; Whitelock et al. 1991, 2000, 1994). Near-infrared mean magnitudes are used. The two curves represent M3 (upper) and an M10 (lower) type stars with increasing mass-loss rates (indicated by squares and labels* $\times 10^{-6}$ $M_{\odot}$*/year), as modelled by Groenewegen & de Jong (1993). The cross indicates the position of an M10 star without mass-loss (*$(H-K)_0 = 0.48$ *and* $(J-K)_0 = 1.34$*). The arrow shows the reddening vector for* $A_{\rm K}$= 1 *mag.*

between intrinsic and interstellar reddening in these colours impossible.

In, both, the $(J-K)_0$ vs. $(K-[12])_0$ and the $(H-K)_0$ vs. $(K-[12])_0$ planes Mira stars are distributed along a broad sequence compared to that seen in the $(J-K)_0$ vs. $(H-K)_0$ plane, as shown in Figs. 4.8 and 4.9.

A comparison with the best fit to the colour-colour sequence of IRAS-selected oxygen-rich AGB stars (van Loon et al. 1998, 1997) shows that in the $(H-K)_0$ vs. $(K-[12])_0$ plane Mira stars lie below that curve, while in the $(J-K)_0$ vs. $(K-[12])_0$ plane there appears no such offset. The offset could be due to water absorption bands in the H band (Frogel & Whitford 1987; Glass et al. 1995), that are found strong in large amplitude variable AGB stars, although we could not find any correlation between colour and variability index for the IRAS stars used by van Loon et al. (Fouque et al. 1992; Guglielmo et al. 1993). The offset might then indicate that for such cold stars the Carter (1990) transformations between the ESO photometry (Fouque et al. 1992; Guglielmo et al. 1993) and the SAAO system (van Loon et al. 1998, 1997) are not adequate.

Mira stars with $0.2 < (H-K)_0 < 3$ mag fit

$$(K-[12])_0 = 4.26(\pm 0.04) + 5.95(\pm 0.17)\,\log(H-K)_0,$$

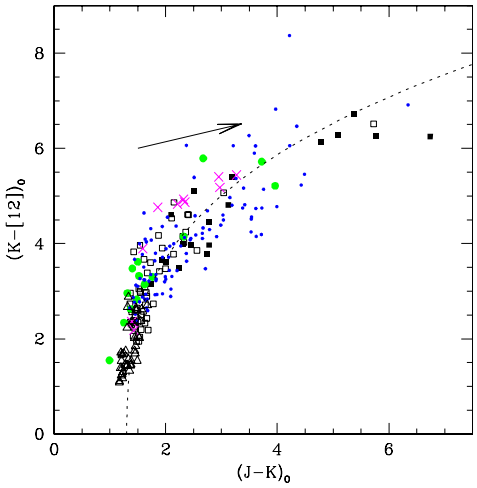

Figure 4.8: *Dereddened colours of infrared-monitored Mira stars (based on the IRAS 12 μm and near-infrared mean magnitudes): in the solar vicinity (filled squares) (Olivier et al. 2001); detected by Hipparcos (open triangles) (Whitelock et al. 2000); toward the South Galactic Cap (open squares) (Whitelock et al. 1994); in the Baade Sgr–I window (big dots) (Glass et al. 1995); in the outer Bulge (small dots) (Whitelock et al. 1991); in the Large Magellanic Cloud (crosses) (Whitelock et al. 1994). The dotted line is the best fit to an IRAS sample of oxygen-rich AGB stars van Loon et al. (1997). The arrow shows the reddening vector for* $A_{\rm K}=1$ *mag.*

with an rms deviation of 0.5 mag. Although we use the SAAO system (Carter 1990), in Appendix A we show that this relation is also valid in the 2MASS photometric system.

4.4 Interstellar extinction and intrinsic colours of the SiO targets

The observed colours of the SiO target stars are shown in Fig. 4.10. For a given $K_{\rm S}-[15]$, the $H-K_{\rm S}$ colours of the SiO target stars are redder than those expected from the colour-colour relation of known Mira stars, and some stars show excess larger than $E(H-K_{\rm S})=1$ mag. This is due to interstellar extinction along the line of sight.

Since observations of Mira stars may suffer from several magnitudes of circumstellar reddening, it not possible to estimate the interstellar extinction toward the SiO target stars by simply assuming an intrinsic colour for a given star.

As seen from Figs. 4.7, 4.8 and 4.9, Mira stars follow near- and mid-infrared colour-colour relations. In the first figure, Fig. 4.7, the reddening vector is paral-

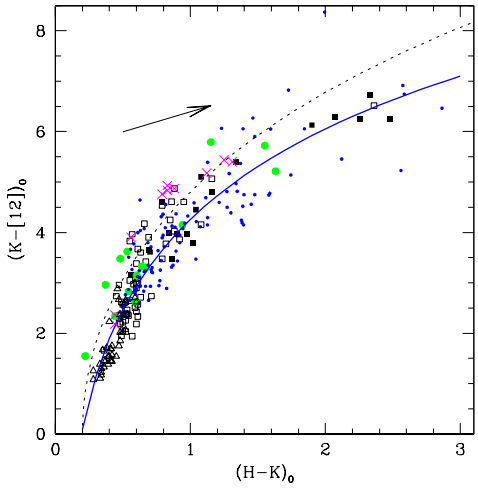

Figure 4.9: *Dereddened colours of infrared-monitored Mira stars, based on the IRAS 12 μm and near-infrared mean magnitudes. Symbols are the same as in Fig. 4.8. The dotted line is the best fit to an IRAS sample of oxygen-rich AGB stars (van Loon et al. 1998). The continuous curve is our best fit for Galactic Mira stars. The arrow shows the reddening vector for* $A_{\rm K}$= 1 *mag.*

lel to the distribution of observed stellar colours and to those of models of AGB stars of increasing shell opacity. In contrast, the reddening vectors in Figs. 4.8 and 4.9 have a slope smaller than that of the distribution of observed stellar points and in principle can permit a separation between interstellar and circumstellar extinction. However, the dispersion of the Mira stars around the colour-colour fiducial sequence is large (0.5 mag), due to the non-contemporaneity of the near- and mid-infrared data and because of the dependence of such relations on metallicity and stellar spectral type. The uncertainty of the interstellar extinction estimates by shifting a star along the reddening vector onto the $H - K_{\rm s}, K_{\rm s} - [15]$ curve is larger than $A_{\rm K_S}$= 1 mag for $K - [15] > 3.5$ mag.

Therefore, to deredden our targets we prefer to use the "field" extinction values (reported in Table 4.3), i.e. we assume that a given SiO target star is located at the distance of the median extinction along the line of sight. Though the dispersion of individual field star extinctions along a given line of sight is considerable (from 0.1 to 0.8 $\sigma_{\rm A_{K_S}}$), the distribution is strongly peaked, especially in the Bulge region. This means also to assume that the SiO targets are located in the region with the highest stellar density along the line of sight. This assumption is justified by the fact that the lifetime of a star on the AGB evolutionary phase is very short ($\sim 5\%$ of the time spent on the helium core burning phase and from 0.1 to 2% of the time spent on the main sequence phase of such a star; Vassiliadis & Wood 1993) and we therefore expect most of the AGB stars to be located in those regions with

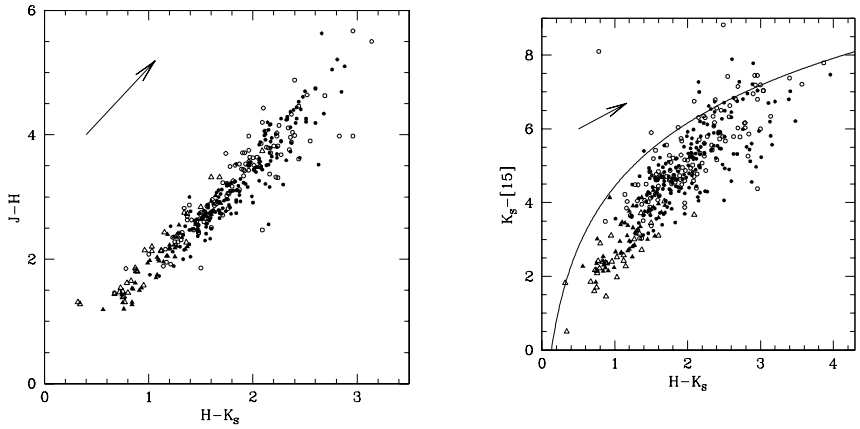

Figure 4.10: Left panel: *2MASS $J - H$ versus $H-K_{\rm S}$ colours. Stars with upper magnitude limits are not shown. Dots and triangles represent objects with $K_{\rm S}$ smaller and larger than 6.0 mag, respectively. Filled and open symbols represent SiO detections and non-detections, respectively. The arrow shows the reddening vector for $A_{\rm K_S} = 1$ mag.* **Right panel:** *2MASS $K_{\rm S}-[15]$ versus $H-K_{\rm S}$ colours. Symbols are as in the left panel. The curve represents the best fit to the colours of known Mira stars (see Sect. 4.3).*

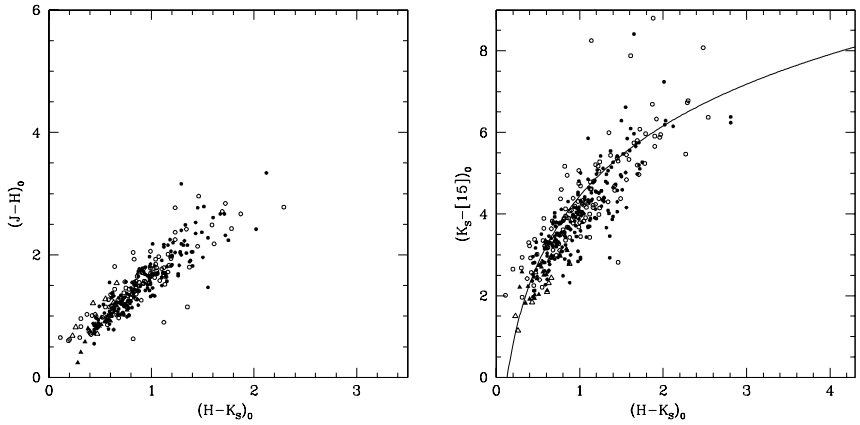

Figure 4.11: Left panel: *Dereddened 2MASS $(J - H)_0$ versus $(H-K_{\rm S})_0$ colours.* **Right panel:** *Dereddened 2MASS $(K_{\rm S}-[15])_0$ versus $(H-K_{\rm S})_0$ colours. Symbols are as in Fig. 4.10. "Foreground objects" have been removed.*

higher stellar density.

The distribution of the SiO targets in the dereddened $(H - K_{\rm S})_0, (K - [15])_0$ diagram (Fig. 4.11) approaches that of known Mira stars. This confirms that the

"field" median extinction is a good approximation of the interstellar extinction for most of the SiO targets and that the SiO targets do mostly belong to the highest stellar density region, i.e. the inner Galaxy. There is still an asymmetry in the distribution of the SiO targets around the fiducial colour line of known Miras, which suggests that we could have underestimated the interstellar extinction for part of the sample. In regions of high extinction, due to their high near-infrared luminosity, Mira-like stars are detectable to larger distances than ordinary field stars. Deeper infrared observations are needed to obtain more accurate extinction estimates (Figer et al. 2004).

4.4.1 "Foreground objects"

Dereddening all observed points in the $(H-K_{\rm s})$ vs. $(J-H)$ diagram (cf. Fig. 4.7) to the $A_{\rm K_S}=0.0$ position, we can measure the total (circumstellar plus interstellar) extinction of each SiO target (Table 4.3). We assumed a stellar photospheric $(J-K_{\rm s})_0$ colour of 1.4 mag and a $H_0-K_{\rm S0}$ colour of 0.5 mag.

The difference of such total extinction estimates from 2MASS and DENIS $J, K_{\rm s}$ data gives an rms of $\Delta A_{\rm K_S}=0.2$ mag, while the estimates from 2MASS $H-K_{\rm s}$ and $J-K_{\rm s}$ colours gives an rms difference of $\Delta A_{\rm K}=0.13$ mag. For only 12 SiO targets we do not have any observed $H-K_{\rm s}$ or $J-K_{\rm s}$ values, and therefore total extinction values are not determined (Table 4.3).

The median interstellar extinction of the field stars surrounding a target star was compared with the individual total extinction of the target star. As expected, on average the target stars show larger total extinctions than their field stars. This is not the case, however, for a group of ~ 50 mostly very bright target stars ($K_{\rm S}<6.0$), at various longitudes, marked with flag 1 in Table 4.3, which have total extinctions lower (a least $1\sigma_{\rm A_{K_S}}$) than the "field" extinction and are therefore likely to be significantly less distant. Thereby the extinction was used to identify foreground objects. We dereddened the "foreground objects" by directly shifting them on the $H, K_{\rm s}, [15]$ colour-colour sequence.

4.5 Intrinsic colours and mass-loss rates

The stellar mass-loss rate is best estimated from measurements of CO rotational lines. The CO emission arises in the circumstellar shell. However, because of confusion with interstellar CO emission it is difficult to obtain such measurements toward stars in the inner Galaxy (Winnberg et al. 1991). Although infrared emission also arises from the stellar photosphere, stellar outflows may be studied from the infrared emission of dust grains which form in the cool circumstellar envelopes. Relations between the infrared colours (e.g. $J-K$, $K-L$, $K-[12]$ or $K-[15]$) of O-rich AGB stars and their mass-loss rate have been established empirically (e.g. Alard et al. 2001; Olivier et al. 2001; Whitelock et al. 1994) and supported by theoretical models (e.g. Ivezíc et al. 1999; Jeong et al. 2003; Groenewegen & de Jong 1993; Ojha et al. 2003).

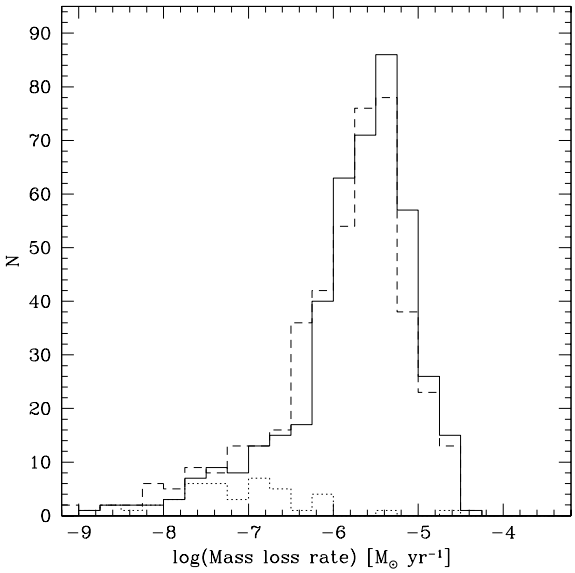

Figure 4.12: *Distribution of mass-loss rates derived from the $K-[15]$ vs. $\dot{M}$ relation Jeong et al. (2003). The continuous line shows the distribution for all SiO targets dereddened using Lutz's extinction law (Curve 3), and the dotted line that of foreground stars. The dashed line is the distribution of all SiO targets using the mid-infrared extinction law of Mathis (Curve 1).*

The empirical relation between the $(K-[15])_0$ colour and the mass loss rate, $\dot{M}$, is very useful to study stars detected in the 2MASS, DENIS, ISOGAL or MSX surveys toward the most obscured regions of the Galaxy.

The uncertainties arising from the variability of the stars and the temporal difference between the $K_{\rm S}$ and 15μm measurements, is somewhat alleviated by using an average of the 2MASS and DENIS $K_{\rm S}$ fluxes and of the ISOGAL and MSX 15μm measurements (Ojha et al. 2003). The remaining r.m.s. uncertainty of the mass-loss rate is thus a factor $\sim$2 for $\dot{M} > 10^{-6}$ M$_\odot$ yr^{-1}.

Following the prescription of Jeong et al. (2003) and Ojha et al. (2003) we obtained mass-loss rates for the SiO targets, the distribution of which is shown in Fig. 4.12. 90% of the sources have implied mass loss rates between 10^{-7} and 2×10^{-5} M$_\odot$ yr^{-1}, with a peak in the range 10^{-6} – 10^{-5} M$_\odot$ yr^{-1}, although the apparent distribution is widened by the uncertainty of the mass-loss–colour relation, by the photometric uncertainty and by the effects of variability. Note that the selection criterion on $(K_{\rm S}-[15])_0$ for the ISOGAL sample completely eliminated sources with $\dot{M} > 10^{-5}$, and that the elimination of OH/IR sources and the criteria on $A-D$ and $C-E$ colours for the MSX sample also considerably reduced the proportion of sources with large mass-loss rates (see Chapter II; Chapter III).

The same results are obtained considering the subsample of targets with the best extinction corrections, i.e. with $\sigma_{\mathrm{A_{K_s}}} < 0.2$ mag. The distribution of the mass-loss rates of the SiO targets with detected SiO maser emission appears similar to that of the SiO targets non-detected (Chapter II).

Adopting Mathis' mid-infrared extinction law rather than Luts's one, the distribution of the mass-loss rates only slightly shift toward lower values (see Fig. 4.12).

4.6 Conclusion

We estimated the interstellar extinction toward each of our 441 SiO target stars. For all 2MASS stars within 2-4′ radius field of each target we shifted the $(J - K_{\mathrm{s}})$ and $(H - K_{\mathrm{s}})$ colour versus K_{s} magnitude along the reddening vector onto the reference red giant branch. The use of both colour-magnitude planes enabled us to obtain a mean extinction for each field and new constraints on the index of the near-infrared extinction power law, α. We found that a value of $\alpha = 1.6$ is inconsistent with the colours of inner Galactic stars, and, taking 47 Tuc as a reference for the RGB, we determine $\alpha = 1.9 \pm 0.1$.

For K_{S}-band extinctions larger than 1.6 mag the 2MASS $(K_{\mathrm{S}}, J - K_{\mathrm{s}})$ CMD yields too low extinction estimates, due to a selection effect from the J-band dropout of more distant sources. The 2MASS $(K_{\mathrm{s}}, H - K_{\mathrm{s}})$ CMD suffers less from this bias.

We reviewed near- and mid-infrared dereddened colour-colour relations of Mira stars and use them to test the quality of the extinction corrections for each SiO target.

Under the assumption that SiO targets are spatially distributed similarly to surrounding field stars, we corrected the photometric measurements of the SiO targets adopting the median extinction of their surrounding field stars. Derredened colours of the SiO targets are not perfectly symmetrically distributed around the fiducial colour-colour line derived from known Mira stars, suggesting that for part of the SiO targets we may still be underestimating the interstellar extinction of up to about 15%. About 50 SiO targets lie significantly in the "foreground" of the mean stellar distribution.

Using the relation between mass-loss rate and $(K_{\mathrm{S}}-15)_0$ colour given by Jeong et al. (2003), we estimated that most of the SiO targets have mass-loss rates in the range 10^{-7} to 10^{-5} $\mathrm{M_\odot\ yr^{-1}}$.

Acknowledgements. The MSX transmission curves were kindly provided by M. Egan. MM thanks P. Popowski, J. van Loon, S. Ganesh, and M. Schultheis for useful discussions on interstellar extinction, and M. Sevenster for her constructive criticism. This paper uses and partly depends on the studies of Mira stars conducted at the SAAO observatory by Patricia Whitelock and her collaborators. The DENIS project was carried out in the context of EARA, the European Association for Research in Astronomy. This publication makes use of data products from the IRAS data base server, from the Two Micron All Sky Survey, from the Midcourse Space Experiment, and from the SIMBAD data base. The work of MM

is funded by the Netherlands Research School for Astronomy (NOVA) through a *netwerk 2, Ph.D. stipend*.

Appendix A: SAAO and 2MASS colours and magnitudes

Transformation equations between the colours and magnitudes measured in the SAAO Carter (1990) and 2MASS photometric systems have been derived by Carpenter (2001) using a list of mostly blue 94 photometric standards. Figure 12 in Carpenter (2001) shows that the differences between magnitudes and colours obtained with the two systems are smaller than 0.15 mag.

Considering that Mira stars have typically a pulsation amplitude in the near-infrared of 1-2 mag and that 2MASS data are from a single-epoch observation randomly taken with respect to the stellar phase, the system transformations have only a secondary effect in the total colour and magnitude uncertainty, when comparing data from 2MASS with data taken with the SAAO telescope.

Since Mira stars are cold objects, molecular absorption bands characterise their infrared spectra and we must exclude that a combination of molecular bands and filter transmissions could generate a different colour transformation for these special class of objects. To address that we looked for 2MASS counterparts of the 104 outer Bulge Mira stars monitored by Whitelock et al. (1994). As demonstrated in Chapter III, Mira stars are among the brightest objects detected in the $K_{\rm s}$ band and therefore the identification of their 2MASS counterparts is straightforward. A number of 101 2MASS counterparts were found within 60″ (mostly within 10″) from the IRAS position. We excluded three sources because they had not unique counterparts (IRAS 17287−1955, IRAS 17030−2801, IRAS 18264−2720).

The differences between the mean magnitudes obtained with SAAO observations (Whitelock et al. 1991) and the single-epoch 2MASS data have a dispersion of up to 0.8 mag.

We obtain the following mean differences:

$$K_{\rm s(2MASS)} - K_{\rm (SAAO)} = -0.15 \pm 0.06 \ {\rm mag};$$
$$(J - K_{\rm s})_{\rm (2MASS)} - (J - K)_{\rm (SAAO)} = -0.14 \pm 0.05 \ {\rm mag};$$
$$(H - K_{\rm s})_{\rm (2MASS)} - (H - K)_{\rm (SAAO)} = -0.06 \pm 0.03 \ {\rm mag}.$$

To verify whether the colour-colour relations found in Sect. 4.3, using data in the SAAO photometric system, hold also when using 2MASS photometry, in Fig. A.1 we plot both SAAO data and 2MASS data for the same sample of Mira stars (Whitelock et al. 1991). No systematic trend is present.

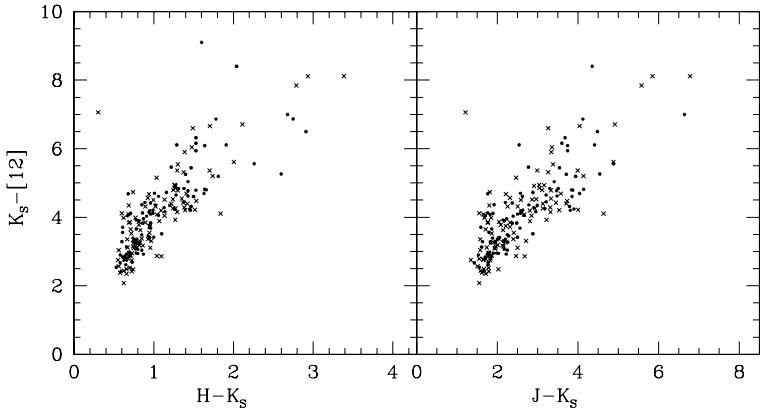

Figure A.1: *Colour-colour plots of Mira stars. The dots indicate average colours of Mira stars obtained from SAAO observations (Whitelock et al. 1991). Crosses indicate colours from single-epoch 2MASS data for the same sample of Mira stars (Whitelock et al. 1991).*

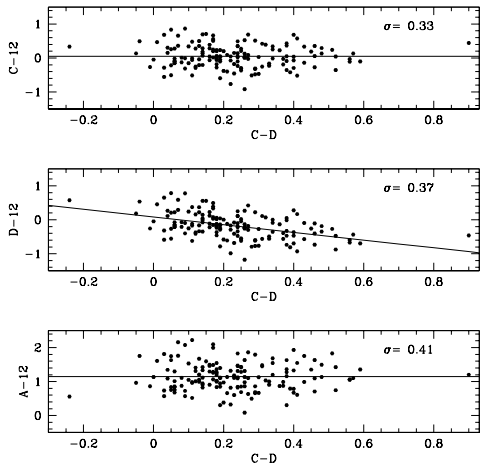

Figure B.2: *Colour-Colour diagrams of our SiO targets. The IRAS 12μm magnitude is defined as* $[12] = -2.5 \log F_{12}[\mathrm{Jy}]/28.3$*. The continuous lines are our best fits.*

Appendix B: IRAS and MSX filters

Most of the past work has been carried out using the IRAS photometry, and therefore the currently available colour-colour relations of Mira stars use mid-infrared data from the IRAS catalogue. A comparison of mid-infrared filters is therefore mandatory to translate old findings into new MSX and ISOGAL colours.

Figure B.2 shows the difference between MSX magnitudes and IRAS 12 μm magnitude for the SiO targets. Note that the D filter excludes the silicate feature

around 9.7 μm, while A and C filters include part of it (see Fig. 4.1). Therefore the $(D-[12])$ colour shows a dependence on the $(C-D)$ colour, which increases when the silicate feature at 9.7 μm starts to be self-absorbed. The $(A-[12])$ and $(C-[12])$ colours do not show any trend with the $(C-D)$ colour. Due to both uncertainties of photometric measurements and source variability the scatter is large, however we derived relations between the A, C, and D and the [12] magnitudes, as follow:
$A-[12] = 1.15 \pm 0.03$ mag
$C-[12] = 0.05 \pm 0.03$ mag
$D-[12] = 0.08(\pm 0.18) - 1.13(\pm 0.05)(C-D)$ mag.

References

Alard, C., Blommaert, J. A. D. L., Cesarsky, C., et al. 2001, ApJ, 552, 289

Bertelli, G., Bressan, A., Chiosi, C., Fagotto, F., & Nasi, E. 1994, A&AS, 106, 275

Blommaert, J. A. D. L., Siebenmorgen, R., Coulais, A., et al., eds. 2003, The ISO Handbook, Volume II - CAM - The ISO Camera

Cardelli, J. A., Clayton, G. C., & Mathis, J. S. 1989, ApJ, 345, 245

Carpenter, J. M. 2001, AJ, 121, 2851

Carter, B. S. 1990, MNRAS, 242, 1

Cioni, M.-R. L., Blommaert, J. A. D. L., Groenewegen, M. A. T., et al. 2003, A&A, 406, 51

Cotera, A. S., Simpson, J. P., Erickson, E. F., et al. 2000, ApJS, 129, 123

Cutri, C. M., Skrutskie, M. F., & Van Dyk, S. 2003, avalaible on line at `http://www.ipac.caltech.edu/2mass/`

Draine, B. T. & Lee, H. M. 1984, ApJ, 285, 89

Drimmel, R., Cabrera-Lavers, A., & López-Corredoira, M. 2003, A&A, 409, 205

Dutra, C. M., Santiago, B. X., & Bica, E. 2002, A&A, 381, 219

Dutra, C. M., Santiago, B. X., Bica, E. L. D., & Barbuy, B. 2003, MNRAS, 338, 253

Egan, M. P., Price, S. D., Moshir, M. M., et al. 1999, AFRL-VS-TR-1999, 1522

Epchtein, N., de Batz, B., Copet, E., et al. 1994, Ap&SS, 217, 3

Ferraro, F. R., Messineo, M., Fusi Pecci, F., et al. 1999, AJ, 118, 1738

Figer, D. F., Rich, R. M., Kim, S. S., Morris, M., & Serabyn, E. 2004, ApJ, 601, 319

Fluks, M. A., Plez, B., The, P. S., et al. 1994, A&AS, 105, 311

Fouque, P., Le Bertre, T., Epchtein, N., Guglielmo, F., & Kerschbaum, F. 1992, A&AS, 93, 151

Frogel, J. A., Tiede, G. P., & Kuchinski, L. E. 1999, AJ, 117, 2296

Frogel, J. A. & Whitford, A. E. 1987, ApJ, 320, 199

Girardi, L., Bressan, A., Bertelli, G., & Chiosi, C. 2000, A&AS, 141, 371

Glass, I. S. 1999, Book Review: Handbook of infrared astronomy (Cambridge U. Press)

Glass, I. S., Whitelock, P. A., Catchpole, R. M., & Feast, M. W. 1995, MNRAS, 273, 383

Groenewegen, M. A. T. & de Jong, T. 1993, A&A, 267, 410

Guglielmo, F., Epchtein, N., Le Bertre, T., et al. 1993, A&AS, 99, 31

He, L., Whittet, D. C. B., Kilkenny, D., & Spencer Jones, J. H. 1995, ApJS, 101, 335

Hennebelle, P., Pérault, M., Teyssier, D., & Ganesh, S. 2001, A&A, 365, 598

Ivezíc, Z., Nenkova, M., & Elitzur, M. 1999, User Manual for DUSTY (Lexington: Univ. Kentucky)

Jeong, K. S., Winters, J. M., Le Bertre, T., & Sedmayr, E. 2003, Proceeding of WS on Mass-Losing Pulsating Stars and their Circumstellar Matter, Sendai, Japan, Y.Nakada & M.Honma (eds), Kluwer ASSL series

Jiang, B. W., Omont, A., Ganesh, S., Simon, G., & Schuller, F. 2003, A&A, 400, 903

López-Corredoira, M., Cabrera-Lavers, A., Garzón, F., & Hammersley, P. L. 2002, A&A, 394, 883

Landini, M., Natta, A., Salinari, P., Oliva, E., & Moorwood, A. F. M. 1984, A&A, 134, 284

Lutz, D. 1999, in ESA SP-427: The Universe as Seen by ISO, Vol. 427, 623

Lutz, D., Feuchtgruber, H., Genzel, R., et al. 1996, A&A, 315, L269

Mathis, J. S. 1990, ARA&A, 28, 37

—. 1998, ApJ, 497, 824

McWilliam, A. & Rich, R. M. 1994, ApJS, 91, 749

Messineo, M., Habing, H. J., Menten, K. M., Omont, A., & Sjouwerman, L. O. 2004a, A&A in preparation (Chapter V)

—. 2004b, A&A, 418, 103 (Chapter III)

Messineo, M., Habing, H. J., Sjouwerman, L. O., Omont, A., & Menten, K. M. 2002, A&A, 393, 115 (Chapter II)

Ojha, D. K., Omont, A., Schuller, F., et al. 2003, A&A, 403, 141

Olivier, E. A., Whitelock, P., & Marang, F. 2001, MNRAS, 326, 490

Omont, A., Gilmore, G. F., Alard, C., et al. 2003, A&A, 403, 975

Price, S. D., Egan, M. P., Carey, S. J., Mizuno, D. R., & Kuchar, T. A. 2001, AJ, 121, 2819

Rieke, G. H. & Lebofsky, M. J. 1985, ApJ, 288, 618

Rosenthal, D., Bertoldi, F., & Drapatz, S. 2000, A&A, 356, 705

Schuller, F., Ganesh, S., Messineo, M., et al. 2003, A&A, 403, 955

Schultheis, M., Ganesh, S., Simon, G., et al. 1999, A&A, 349, L69

Stanek, K. Z. 1998, Using the DIRBE/IRAS All-Sky Reddening Map to Select Low-Reddening Windows Near the Galactic Plane, preprint [astro-ph/9802307]

Udalski, A. 2003, ApJ, 590, 284

van de Hulst, H. C. 1946, Optics of spherical particles. (Amsterdam, Drukkerij J. F. Duwaer, 1946.), 1

van Loon, J. T., Gilmore, G. F., Omont, A., et al. 2003, MNRAS, 338, 857
van Loon, J. T., Zijlstra, A. A., Whitelock, P. A., et al. 1998, A&A, 329, 169
—. 1997, A&A, 325, 585
Vassiliadis, E. & Wood, P. R. 1993, ApJ, 413, 641
Wainscoat, R. J., Cohen, M., Volk, K., Walker, H. J., & Schwartz, D. E. 1992, ApJS, 83, 111
Whitelock, P., Feast, M., & Catchpole, R. 1991, MNRAS, 248, 276
Whitelock, P., Marang, F., & Feast, M. 2000, MNRAS, 319, 728
Whitelock, P., Menzies, J., Feast, M., et al. 1994, MNRAS, 267, 711
Whitelock, P. A., Feast, M. W., van Loon, J. T., & Zijlstra, A. A. 2003, MNRAS, 342, 86
Winnberg, A., Lindqvist, M., Olofsson, H., & Henkel, C. 1991, A&A, 245, 195